

Article

Investigation of Punch Shape and Loading Path Design in Hydro-Flanging Processes of Aluminum Alloy Tubes

Yeong-Maw Hwang *, Hong-Nhan Pham and Hiu-Shan Rachel Tsui

Department of Mechanical and Electro-Mechanical Engineering, National Sun Yat-Sen University, Lien-Hai Rd., Kaohsiung 804, Taiwan; d033020006@nssysu.edu.tw (H.-N.P.); m093020096@nssysu.edu.tw (H.-S.R.T.)

* Correspondence: ymhwang@mail.nssysu.edu.tw; Tel.: +886-7-525-2000

Abstract: Hydro-joining is composed of hydro-piercing, hole flanging and nut-inlaying processes. In this study, a new hydro-flanging process combining hydro-piercing and hydro-flanging is proposed. An internal pressured fluid is used as the supporting medium instead of a rigid die. Three kinds of punch head shapes are designed to explore the thickness distribution of the flanged tube and the fluid leakage effects between the punch head and the flanged tube in the hydro-flanging process. A finite element code DEFORM 3D is used to simulate the tube material deformation behavior and to investigate the formability of the hydro-flanging processes of aluminum alloy tubes. The effects of various forming parameters, such as punch shapes, internal pressure, die hole diameter, etc., on the hydro-flanged tube thickness distributions are discussed. Hydro-flanging experiments are also carried out. The die hole radius is designed to make the maximum internal forming pressure needed smaller than 70 MPa, so that a general hydraulic power unit can be used to implement the proposed hole flanging experiments. The flanged thickness distributions are compared with simulation results to verify the validity of the proposed models and the designed punch head shapes.



Citation: Hwang, Y.-M.; Pham, H.-N.; Tsui, H.-S.R. Investigation of Punch Shape and Loading Path Design in Hydro-Flanging Processes of Aluminum Alloy Tubes. *Metals* **2021**, *11*, 636. <https://doi.org/10.3390/met11040636>

Academic Editor: Umberto Prisco

Received: 15 March 2021

Accepted: 12 April 2021

Published: 13 April 2021

Publisher's Note: MDPI stays neutral with regard to jurisdictional claims in published maps and institutional affiliations.



Copyright: © 2021 by the authors. Licensee MDPI, Basel, Switzerland. This article is an open access article distributed under the terms and conditions of the Creative Commons Attribution (CC BY) license (<https://creativecommons.org/licenses/by/4.0/>).

Keywords: tube hydroforming; hydro-flanging; punch head shape; finite element analysis; aluminum alloy

1. Introduction

Nowadays, energy saving and carbon dioxide reduction have become important issues in the world, especially in aerospace and transportation fields. Tube hydroforming (THF) processes have been applied to manufacture lightweight parts in various fields, such as bicycles, automobiles and aerospace industries. Compared with conventional metal forming processes, tube hydroforming has some merits, such as reductions in workpiece cost, tool cost and product weight. THF can also improve structural stability and increase strength and stiffness of the formed parts, such as front and rear axles, exhaust system components, body frames, etc. [1,2] Recently, tube hydroforming processes sometimes incorporate piercing, flanging, or joining processes to become hydro-piercing, hydro-flanging, or hydro-joining, which are more efficient compared with a single process and can reduce the total weight of the final product.

Some research concerning hydro-piercing and hydro-flanging processes of sheets or tubes have been presented. For example, Fracz et al. [3] investigated the effect of punch geometry on the sheet thickness distribution during hole-flanging process. Three different punch geometries: cylindrical (flat-bottomed), hemispherical and conical, were used in the experiment, as well as in numerical simulation. The results of experimental investigations were compared with the FE simulation results. Kacem et al. [4] used a conical punch to characterize and predict numerically the limits of the hole flanging process arising from material failure for two different aluminum sheets. Then, a fracture criterion based on local strain measures in tension has been identified for both materials. Finally, numerical predictions of the strain limits obtained from successful parts were compared to experimental results. Liu et al. [5] proposed a new hybrid technology of hole

hydro-piercing-flanging processes. The influence of punch shape on geometrical profile and quality of holes was investigated by experiments and simulations using a punch of different shapes at the transition zone. The results showed that the geometrical dimensions of the roll-over depth, straight-ring zone height and thickness distributions varied with punch shapes. Finally, the mechanism of hydro-piercing-flanging process affected by the punch shape was clarified from the stress and strain distributions by the finite element analysis.

Thipprakmas et al. [6] proposed a fine blanked-hole (FB-hole) flanging process to investigate the deformation of a sheet by the finite element method. The FE simulation results of the flanged shapes were compared with experimental results and good agreement was found. The results verified that the FB-hole flanging process resulted in better-flanged shapes and flangeability than those obtained by the conventional-hole flanging process. Mizumura et al. [7] investigated the influence of internal pressure on hydro-burring after hydro-piercing of steel tubes. They found internal pressures during hydro-burring have large effects on the formability of burring processes. The hydroformed component can be joined to another part with the thread tapped at the hydro-burring portion. However, it is difficult to tap thin-ring parted tubes. Therefore, they also developed a new nut-inlaying method in a hydroformed component, by which thin-ring parted hydroformed components can also be joined to other parts using this nut-inlaying method. Mizumura et al. [8] developed a method of hydro-burring, wherein a hole made by hydro-piercing was expanded while the internal pressure was maintained. It became possible to join formed parts to others with bolts by tapping screw threads to the hole or inlaying a nut there. Choi et al. [9] analyzed the tube deformation behavior surrounding a hole produced by a hydro-piercing process. They investigated both experimentally and analytically the relationship between the deformation radius and the roll-over under different punch diameters and internal pressures.

One of the present authors has published a series of works related to tube hydroforming processes [10–12]. For example, Hwang and Wu [10] proposed a compound forming process including crushing, hydroforming and calibration, for hydroforming a rectangular cross-sectional tube of aluminum alloys A6061-O. Using the proposed compound forming processes and an appropriate loading path, a uniform thickness distribution in the formed tube, a lower internal pressure and a smaller clamping force were obtained compared with the tradition hydroforming process. Hwang et al. [11] used finite element simulations and experiments to investigate the effects of punch shape and various parameters such as punch strokes, internal pressures, etc., on the pierced hole surface characteristics in a tube hydro-piercing process of SPFC590Y carbon steel tubes. The deformation mechanisms for obtaining a better surface characteristic were also discussed. Hwang and Tsai [12] proposed a tube hydroforming process with a novel movable die concept and loading path design to manufacture irregular bellows with small thinning ratios in the formed product. Two kinds of feeding types were proposed to make the maximal thinning ratio in the formed bellows as small as possible. A finite element simulation software “DEFORM 3D” was used to analyze the plastic deformation of the tube within the die cavity using the proposed movable die design. Using the movable die design with an appropriate die gap width, the internal forming pressure needed can be reduced to only one-sixth of the internal pressure needed without the movable die design.

Park et al. [13] proposed an advanced sealing system to prevent fluid leakage during the hydroforming process. The advanced sealing system was composed of a die spring, cylindrical sleeve and punch with end fillet. With the proposed sealing system, the circumference of the tube end became more tightly sealed by the axial pressure between the punch and sleeve and the axial pressure increased with increasing axial feeding. The feasibility of the proposed sealing system was experimentally confirmed by hydroforming a non-axisymmetric complicated part. Yu et al. [14] introduced a quantitative method to evaluate effects of crack size and material anisotropy on edge stretchability with an index of effective failure strain ratio during punching of sheet metals. Numerical studies were conducted to

investigate the interaction effect of cracks and anisotropy on the edge stretchability during hole stretching. The results showed that cracks are prone to appearing along the direction with the lowest r -value within the sheet plate. Punching and hole-expansion experiments using Dual Phase steel were conducted to validate the conclusions. Kumar et al. [15] used finite element simulations and experiments to investigate the effect of punch head profiles on deformation behavior of AA5052 alloy sheet in stretch-flanging processes. Six different punch geometries were used. The simulative and experimental results showed that the circumferential strain, radial strain and punching load are minimum with a hemispherical punch profile as compared to other punch profiles.

Material behavior modellings influence the design of processes, tools and the final products in metal forming or machining processes. Dixit et al. [16] presented a comprehensive review of various approaches of material behavior modellings. Metal forming processes, traditional machining processes and non-traditional machining processes were all considered in this review paper. Different material models were compared with respect to their suitability for the design of processes, tools and products. Del Pozo et al. [17] proposed a methodological scheme for a reduction of both the try-out and lead-time of complex dies. From the finite element simulation of the press/tool deflection during the stamping process, the best design of high-cost dies/punches was recommended. Fernández-Abia et al. [18] proposed a mechanistic model for cutting force prediction. The effect of the edge force due to the rounded cutting edge was also considered in their model. In addition, a set of machining tests were carried out to obtain the specific force coefficients expressions for austenitic stainless steels using the mechanistic approach at high cutting speeds. The results were validated by comparing the values estimated by the model with the ones obtained by experimentation.

The present authors have proposed a punch design concept in hydro-reaming and hydro-flanging of aluminum alloy tube [19]. In this study, a new hybrid forming process combining hydro-piercing and hydro-flanging of a tube is proposed. The formability of a round hole flanging process of aluminum alloy A6063 tubes is investigated numerically and experimentally. The effects of punch geometries, die hole radius and internal pressure on the formability of the hydro-flanging process and the tube thickness distributions at the ring zone after hydro-flanging are discussed. The forming conditions for obtaining sound product with a ring zone over 3 mm thick and without oil leakage at the interface between the tube and punch are also explored.

2. Finite Element Modelling

2.1. Geometric Configurations during Hydro-Flanging

The specimens for the tensile test were cut using wire-cutting directly from the aluminum alloy tube in the longitudinal direction with the ASTM standard dimensions [20]. Then, tensile tests were conducted at constant strain rates of 0.1 and 0.01 s⁻¹ at room temperature using an INSTRON universal testing machine. After the tensile tests, the recorded loads and elongations of the specimens were transferred into true stresses and true strains, respectively, as shown in Figure 1. The yielding stress with the 0.2% offset method is about 40 MPa. At small strains, the two curves almost overlap, whereas at large strains, there is about a 2% difference in the flow stresses. The flow stresses at the two different strain rates are adopted in the finite element simulations.

The geometric configurations between the tube, punch and die before a hydro-flanging process are shown in Figure 2. The outer surface of a tube is supported by a die with a hole, through which a punch is moved forward to implement piercing and flanging processes. The inside of the tube is filled with a high pressure fluid, acted as a supporting media to increase the process formability and make the formed product shape and dimensions meet the requirements as can as possible.

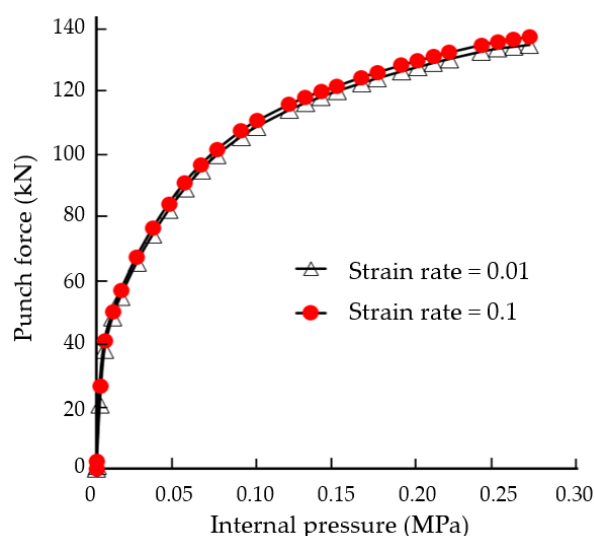


Figure 1. Stress-strain curves of aluminum alloy tube A6063.

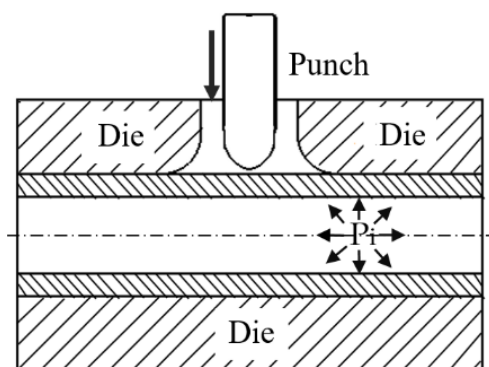


Figure 2. Geometric configurations of tube, die and punch in hydro-flanging.

The whole hydro-flanging process is divided into two stages: (1) free bulging and (2) hole flanging, as shown in Figure 3a,b, respectively, where r_h and r_p are the radii of the die hole and the punch head, respectively. P_i is the internal pressure, R is the die fillet radius, t is tube thickness and H_p is the height of the punch head. In Figure 3a, as the tube is bulged upward with a distance H_b in z direction, the punch starts to move downward to implement hole flanging stage, as shown in Figure 3b. t_0 , t_1 and t_2 are the thicknesses of the flanging region at positions of s_0 , s_1 and s_2 , respectively, which correspond to z coordinates of z_0 , z_1 and z_2 , respectively. If the punch fillet radius ρ (shown in Figure 3a) and other forming conditions are not appropriately set, the thickness t_0 at the tip of the punch head (zone A) becomes close to that at zone B and the tube breakage probably occurs in zone B. The punch head shape is an important factor influencing the position of tube breakage greatly. The punch head aspect ratio is defined as H_p/r_p , which is related with the punch fillet radius ρ . As r_p is set as 3.45 mm, then three different punch heights of $H_p = 4, 4.5$ and 5 mm will correspond to three different punch fillet radii of $\rho = 4.04, 4.68$ and 5.41 mm, respectively.

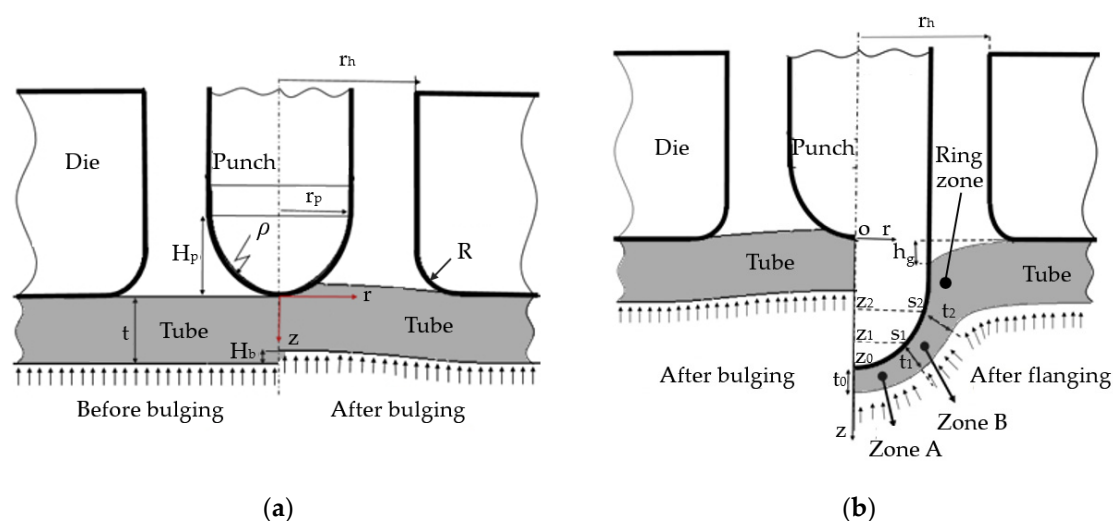


Figure 3. Schematic diagrams in different stages. (a) Free bulging stage; (b) Hole flanging stage.

2.2. Finite Element Simulations in Hydro-Flanging

Table 1 shows the forming conditions used in the finite element simulations in hole hydro-flanging processes. The aluminum alloy A6063 tube is set as an elasto-plastic material, whereas die and punch are set as rigid body in the finite element simulations. The tube outer diameter d_0 is 50.8 mm and the initial thickness t is 3 mm. Three punch heights of 4, 4.5 and 5 mm are designed. Three die hole radii r_h are 3.5 mm, 5 mm and 6.5 mm. Three internal pressures of 30, 50 and 70 MPa are selected. The forming temperature is set as 25 °C. The die fillet radius is set as 0.2 mm.

The loading paths of internal pressure and punch positions for free bulging and flanging stages are shown in Figure 4. At stage 1, the internal pressure is increased from 0 to P_{i1} . At stage 2, the punch starts to move downward to implement flanging stage with punch speed of 1 mm/s.

Table 1. Forming conditions used in finite element simulations.

| Object | Dimension or Property |
|---------------------------------|---------------------------|
| Tube material | A6063-T0 (Elasto-plastic) |
| Tube outer diameter d_0 (mm) | 50.8 |
| Tube initial thickness t (mm) | 3 |
| Punch material | Rigid |
| Punch radius r_p (mm) | 3.45 |
| Punch head height H_p (mm) | 4.5 |
| Die material | Rigid |
| Die inner diameter (mm) | 50.8 |
| Die hole radius r_h (mm) | 3.5 |
| Internal pressure P_i (MPa) | 50 |
| Temperature (°C) | 25 |

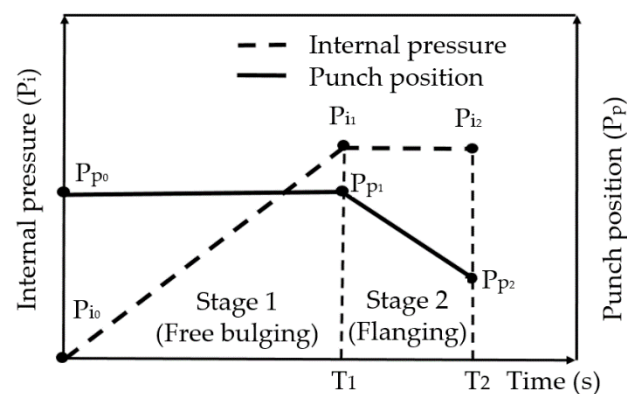
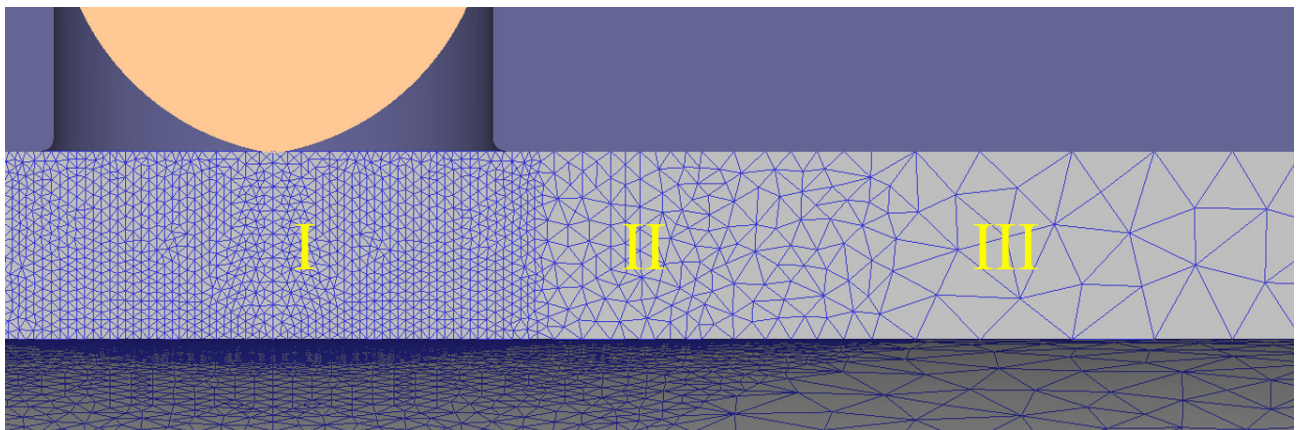


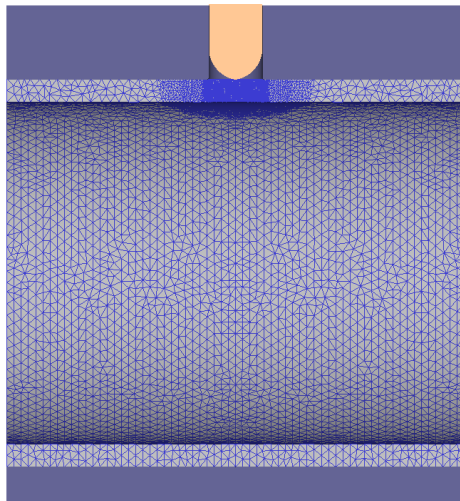
Figure 4. Loading path for internal pressurization and punch position.

An implicit and static FE code “DEFORM 3D” was adopted to analyze the plastic deformation pattern of an aluminum alloy tube during hydro-flanging processes. The finite element code is based on the flow formulation approach using an updated Lagrange procedure. At first, the geometries of the objects are constructed using a commercial software Solidworks. Then, DEFORM 3D is used to implement the simulation of hydro-flanging processes. The punch and die are regarded as rigid bodies and the tube is elasto-plastic. The flow stresses of the tube material are considered as a function of strain and strain rate. The stress-strain curves at strain rates of 0.1 and 0.01 s^{−1} shown in Figure 1 were input in the finite element modelling. The coulomb friction model was adopted at the interfaces between the tube and the punch head and the die. For a dry friction interface, the friction coefficients are usually assumed as 0.1–0.2. Because of different surface roughness at the punch head and the die, friction coefficients of 0.15 and 0.2 were assumed for the interfaces in contact with the punch and tube, respectively. The constant shear friction model is usually adopted at the contact surfaces in warm forming or hot forming processes for avoiding overestimate in the friction stresses. The length of the tube is 60 mm. Due to symmetry on the left-right and front-back side, only one quarter of the objects was adopted in the simulations to save the simulation time. One quarter of the tube having totally about 50,000 elements is divided into three zones, which have different element size ratios, set as 0.2, 0.4 and 1 for zones I, II and III, respectively, as shown in Figure 5a. The tube material in zone I just below the punch head will undergo severest plastic deformation; thus, a smallest element size ratio was set in this region. It is known that there are over ten layers of meshes in zones I and II in the thickness direction of the tube. The mesh configurations before and after hydro-flanging are shown in Figure 5b,c, respectively. The effects of various forming conditions on the thickness distributions at the flanging region and the punch force will be discussed in the next section.

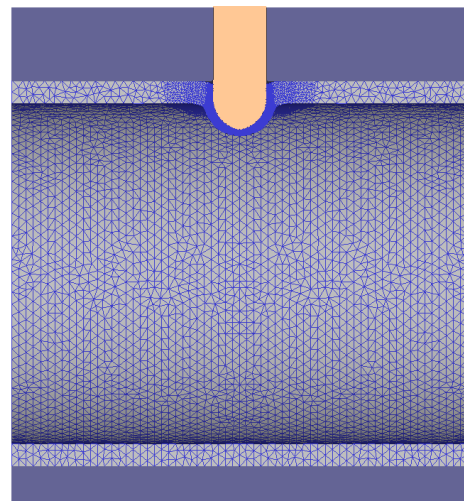
Convergence analyses for simulation results were implemented to understand the ranges of the simulation result errors. Finite element simulations with different total element numbers were conducted. The effects of total element number on the maximal punch force during hydro-flanging processes are shown in Figure 6. Clearly, the relative differences in the maximal punch forces decrease to within 0.5% as the total element number increases to 40,000 elements. Accordingly, approximately 50,000 tetrahedron elements were set for the tube object in the following finite element simulations.



(a)



(b)



(c)

Figure 5. Mesh configurations before and after hydro-flanging. (a) Element size ratios of 0.2, 0.4 and 1 for zones I, II and III, respectively; (b) Before forming; (c) After forming.

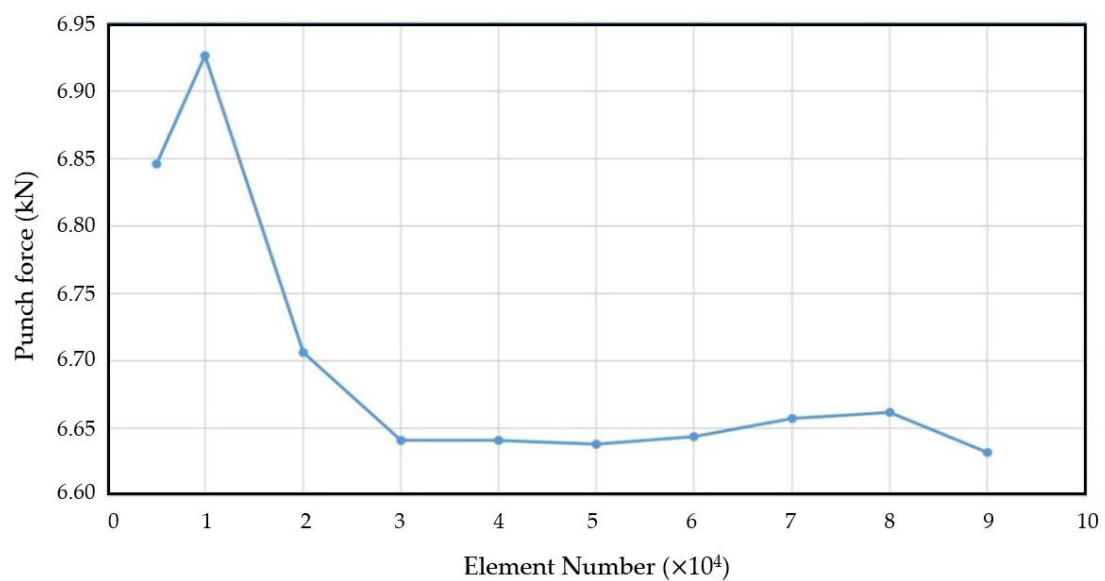


Figure 6. Effects of total element number on maximal punch forces.

3. Simulation Results and Discussion

3.1. Thickness Distributions at Flanging Region

It is important to obtain a thick and long ring zone after hydro-flanging processes for subsequent nut-laying processes. In order to achieve this objective, the tube is first bulged up in the free bulging stage with a distance of H_b to fill the hole vacancy, which can increase the thickness at the ring zone after the flanging stage. Secondly, the forming conditions in the flanging stage, especially the punch shape is designed to make the thickness distributions at the flanging region with $t_2 > t_1 > t_0$. In this way, the fracture position of the tube occurs at the bottom of the punch head, which can make the ring zone become thicker and longer eventually. If the thickness distribution is $t_2 > t_0 > t_1$, or $t_0 > t_2 > t_1$, fracture will probably occur in zone B and the fluid sealing function between the punch head and flanging region may fail. For the case of $t_2 > t_1 > t_0$ at the flanging region, fracture probably occurs at the bottom of the punch head (zone A) and due to the elastic recovery of the tube at the flanging region and the internal pressure compression, the flanging region can stick to the punch head surface and prevent liquid leakage for an effective sealing function.

Figure 7a,b show the simulation results of the thickness distributions with a short and long punch head heights, respectively, at a high internal pressure of $P_i = 70$ MPa and a stroke of 6.5 mm. The die hole radius is $r_h = 3.5$ mm, slightly larger than the punch radius $r_p = 3.45$ mm. From Figure 7a, it can be seen that the thickness of flanging region is quite uniform and there is a small gap or roll-over of $h_g = 0.4$ mm. Fracture probably occurs at zone B, as the punch moves downward further. That is because the downward drawing force from the surface friction between the tube and punch is quite large, which makes the material close to the lower punch head is pulled downward by the punch. Meanwhile, the tube material close to the upper punch head is pushed up by the high internal pressure. These two effects cause the material in zone B to elongate and, finally, fracture occurs at zone B. Figure 7b shows the effects of a longer punch ($H_p = 5$ mm) on the thickness distribution at the flanging region. Clearly, the thickness t_0 at the bottom of flanging region is thinnest and even necking occurred there. The thickness t_2 close to the upper punch head is much larger than t_0 . If the punch moves downward further, fracturing will happen at the bottom of the punch head (zone A). That is because a sharp punch head makes the tube material more easily to flow upward and make the tube thicker close to the upper punch head. Accordingly, the thickness ratio of t_2/t_0 is an important factor for predicting the occurrence of fracturing within zone A or zone B. On the other hand, in Figure 7b, the gap or roll-over is almost zero, because of the high internal pressure pushing the tube upward to contact with the die tightly. A longer ring zone with a smaller roll-over is beneficial for subsequent nut-inlaying processes.

Table 2 shows thickness distributions at the flanging region for different punch heights and internal pressures. Figure 8 shows the effects of punch height H_p and internal pressure P_i on the thickness ratio t_2/t_0 at the flanging region at a punch stroke of 5 mm. As stated earlier, the thickness ratio of t_2/t_0 is the larger the better. A larger t_2/t_0 can make the fracture occurring at the bottom of the flanging region, have a good sealing effect and obtain a longer ring zone. From Figure 8, it is known that the thickness ratios t_2/t_0 obtained with a larger punch height (an acute punch head) are larger than those using a smaller punch height (a blunt punch head), which means an acute punch head is helpful for obtaining a longer ring zone. As $H_p = 5$ mm, a larger internal pressure can increase the thickness ratio, whereas, as $H_p = 4$ mm, a larger internal pressure decreases the thickness ratio. It can be concluded that among the 9 cases, $H_p = 5$ mm and $P_i = 70$ MPa are better conditions to obtain a thick and long ring zone after hydro-flanging. The mechanism for an acute or sharp punch head that can obtain a better ring zone is explained in the following figures.

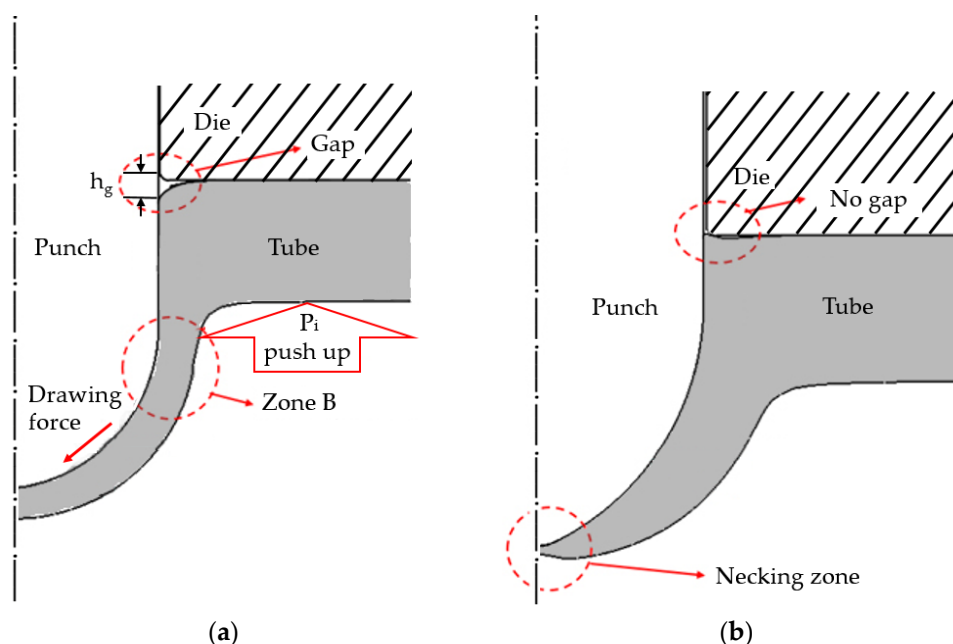


Figure 7. Hydro-flanging results for different punch head heights at $P_i = 70$ MPa. (a) $H_p = 4$ mm; (b) $H_p = 5$ mm.

From Figure 8, it is known that the internal pressure slightly influences the thickness ratio, whereas the punch head height influences the thickness ratio significantly. In order to obtain the desired thickness ratio or deforming shape of the flanging region, punch shape design is more effective than internal pressure design. The relationships between the forming conditions and the thickness ratio or the gap height are quite complicated. For example, in Figure 8, the tendency of the effects of the internal pressure on the thickness ratio is different for different punch head heights. From the simulation results obtained in this paper, it is difficult to propose an empirical equation to present the relationships between the forming conditions and the thickness ratio or the gap height. In the future, a more detailed plan for selections of various forming parameters will be carried out to obtain more detailed simulation results and then some empirical equations can be proposed.

Table 2. Thickness distributions at flanging region for different punch head heights and internal pressures.

| Punch Height (H_p) | Internal Pressure (P_i) | t_2 ($Z_2 = 2.5$ mm) | t_1 ($Z_1 = 3.75$ mm) | t_0 ($Z_0 = 5$ mm) | t_2/t_0 |
|------------------------|-----------------------------|----------------------------|-----------------------------|--------------------------|-----------|
| 4 mm | 30 MPa | 1.918 | 1.750 | 1.549 | 1.238 |
| | 50 MPa | 1.686 | 1.627 | 1.420 | 1.187 |
| | 70 MPa | 1.523 | 1.608 | 1.456 | 1.046 |
| 4.5 mm | 30 MPa | 2.076 | 1.664 | 1.206 | 1.721 |
| | 50 MPa | 1.842 | 1.600 | 1.100 | 1.675 |
| | 70 MPa | 1.760 | 1.563 | 1.031 | 1.707 |
| 5 mm | 30 MPa | 2.117 | 1.669 | 0.990 | 2.138 |
| | 50 MPa | 1.932 | 1.597 | 0.876 | 2.205 |
| | 70 MPa | 1.846 | 1.545 | 0.810 | 2.279 |

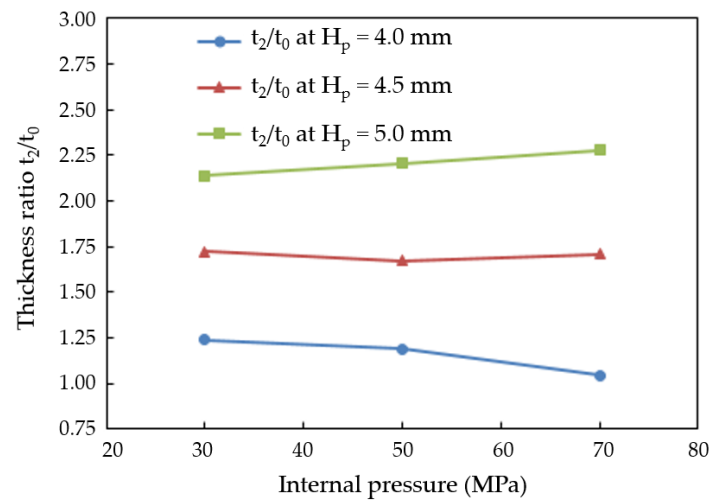


Figure 8. Effects of punch height and internal pressure on thickness ratio at zone B.

Figure 9 shows the effects of internal pressures on the roll-over or gap height with a blunt punch head of $H_p = 4$ mm and a large die hole radius of $r_h = 6.5$ mm. In Figure 9a, at a lower internal pressure, a thicker flanging region and a larger gap $h_g = 1.0$ are obtained. Meanwhile, at a higher internal pressure in Figure 9c, a thinner flanging region and a negative gap height $h_g = -0.44$ mm are obtained. At a lower internal pressure, the tube material is pulled downward by the blunt punch head, which results in a thicker flanging region and a positive gap height. At a higher internal pressure, the tube material is bulged upward, which results in a thinner flanging region and a negative gap height. At an intermediate internal pressure of $P_i = 50$ MPa, shown in Figure 9b, an almost zero gap height is obtained, which geometry is beneficial for subsequent inlaying joining processes.

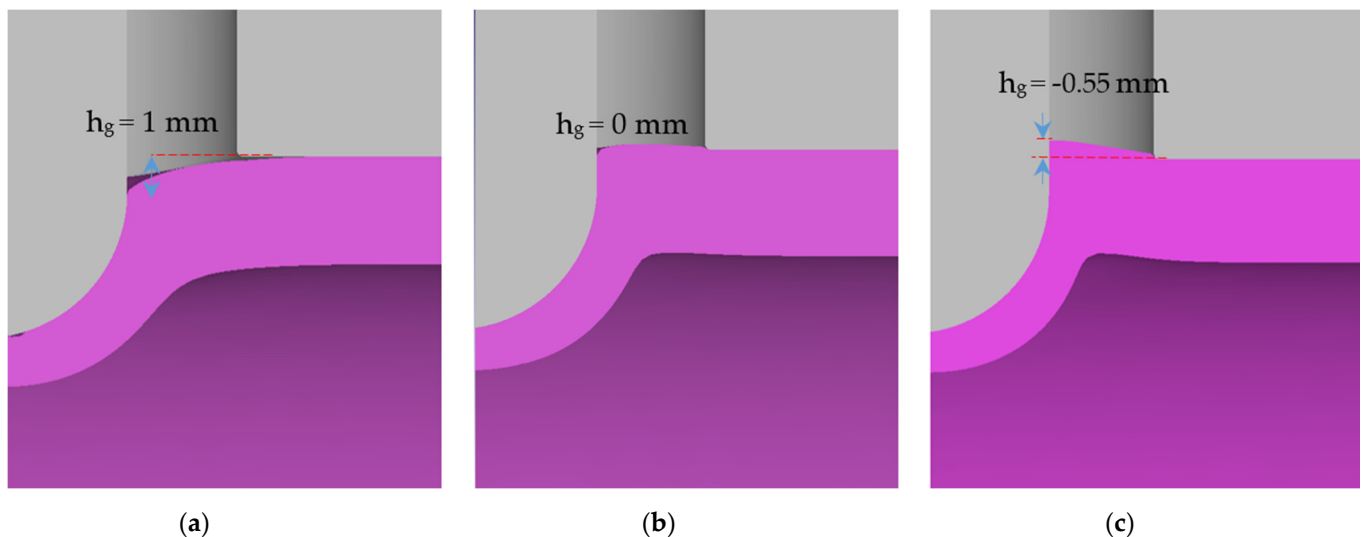


Figure 9. Effects of internal pressure on gap height with larger die hole radius. (a) $P_i = 30$ MPa; (b) $P_i = 50$ MPa; (c) $P_i = 70$ MPa.

Figure 10 shows the effects of die hole radius on the roll-over or gap height with a blunt punch head of $H_p = 4$ mm and an internal pressure of $P_i = 50$ MPa. It can be seen from the figure that as the die hole radius r_h increases, much more tube materials can be raised by the internal pressure to the hole cavity of the die and a smaller roll-over or gap is obtained. However, if the internal pressure is larger than 50 MPa, the gap height h_g may become negative, which is not beneficial for subsequent inlaying processes. The target of

this hydro-flanging process is obtaining a zero-gap height ($h_g = 0$) and making the ring zone as thick as possible.

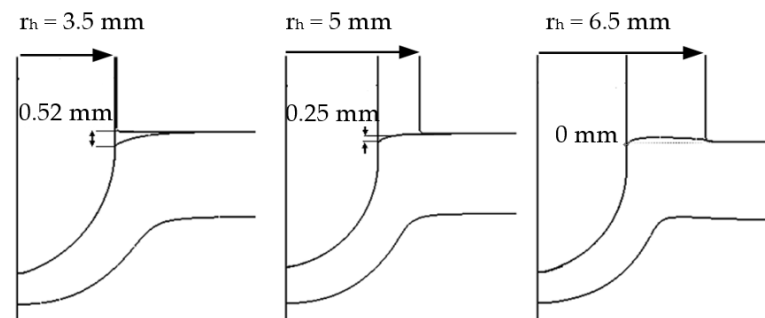


Figure 10. Effects of die hole radius on gap height under $P_i = 50$ MPa.

3.2. Punch Load Variations

Figure 11 shows the punch load variations with different punch height H_p at $P_i = 50$ MPa and $r_h = 5$ mm. The punch load is determined by the punch contact area and the tube thickness at the flanging region. At the early stage, the punch contact area increases with the punch stroke; thus, the punch load increases with the stroke. As the stroke reaches about 4~5 mm, the whole punch head surface is in contact with the tube. After that, the tube at the flanging region continuously becomes thinner. Accordingly, the load begins to decrease at the late stage. For a long punch head (larger H_p), the projected area is smaller than that obtained with a short punch head (smaller H_p) at the same stroke, thus, a smaller punch load is obtained with a larger H_p . The stroke corresponding to the peak value with a larger H_p occurs later, that is because the whole contact surface at the punch head reaches the maximum at a later moment compared with a smaller H_p . At the final stage, the fracture point with $H_p = 5$ mm occurs at the bottom of the flanging region (zone A), whereas the fracture point with $H_p = 4.5$ mm occurs at the middle of the flanging region (zone B). The average thickness with $H_p = 5$ mm is thicker than that with $H_p = 4.5$ mm, thus, the punch load at the fracture point with $H_p = 5$ mm is slightly larger than that with $H_p = 4.5$ mm.

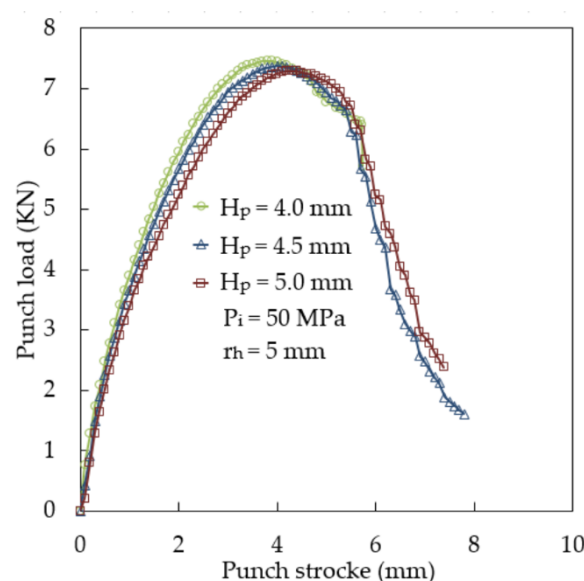


Figure 11. Punch load variations for different punch heights.

Figure 12 shows the punch load variations for different internal pressures P_i at $H_p = 4.5$ mm and $r_h = 5$ mm. Clearly, the punch load increases with the internal pressure,

because a larger punch load is needed to counterbalance the internal pressure imposed on the tube inner surface. At a higher pressure, more tube material is pushed up and more tube material is in contact with the punch head; thus, the punch load reaches its peak value earlier than that at a lower pressure.

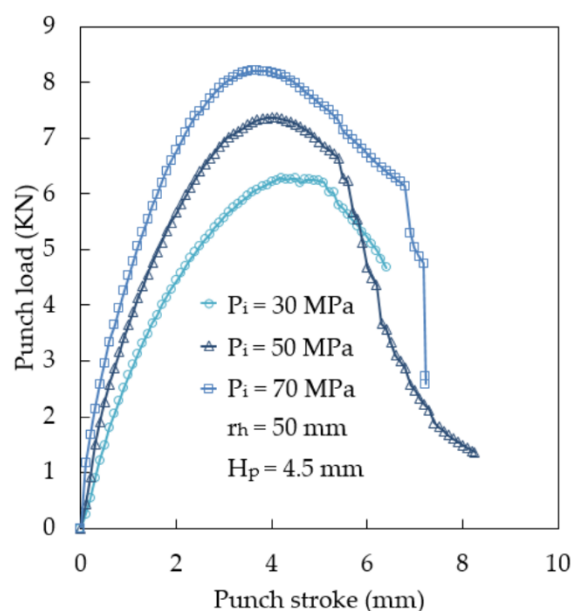


Figure 12. Punch load variations for different internal pressures.

4. Experiments of Hydro-Flanging of Aluminum Alloy Tubes

Aluminum alloy tubes A6063 were annealed before hydro-flanging experiments. The annealing temperature was kept at 420 °C for 3 h, then reduced at a cooling rate of 30 °C/h until 260 °C and, finally, cooled down to room temperature naturally. Figure 13 is the cross-sectional drawing of the die set for hydro-flanging experiments. Table 3 is the list of the components used in the die set. A tube (1) was first put into the die cavity and then 2 nuts (9) was screwed to pull two mandrels (4) backward. Two rubber rings (6) were squeezed by the mandrels (4) and two steel rings (5) to dilate laterally to achieve oil sealing functions.

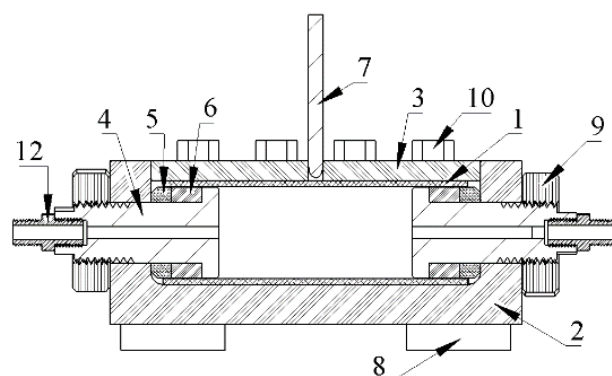
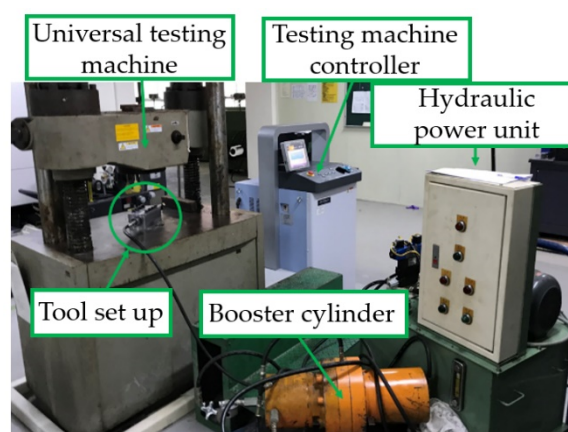
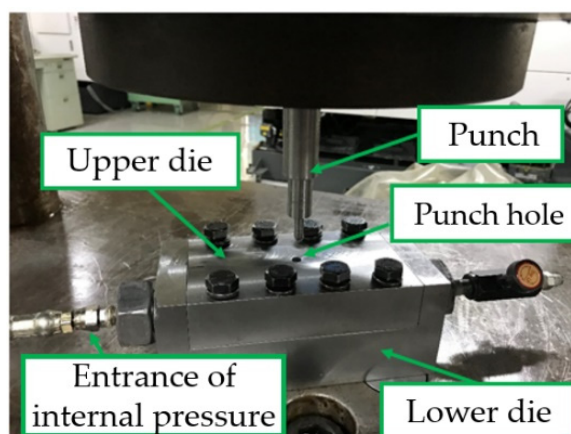


Figure 13. Cross sectional drawing of die set for hydro-flanging.

Table 3. List of die components.

| No. | Component | No. | Component |
|-----|---------------|-----|-----------------|
| 1 | Aluminum tube | 7 | Punch |
| 2 | Lower Die | 8 | Positioning pin |
| 3 | Upper Die | 9 | Nut (M30) |
| 4 | Mandrel | 10 | Screw (M12) |
| 5 | Steel ring | 11 | Screw (M6) |
| 6 | Rubber ring | 12 | Hose connector |

Figure 14 shows the main apparatus used in the hydro-flanging experiments. A universal testing machine was used to control the punch movement. A hydraulic system was used to supply oil source and a booster cylinder was designed to make the output pressure reach as high as 100 MPa. The die set, shown in Figure 15, was positioned on the working table of the universal test machine. After the tube was pressurized to the set value, the punch controlled by the universal testing machine started to move downward to implement hydro-flanging experiments. The main purpose of hydro-flanging experiments is to validate the finite element modelling and the punch head shape design concept. Thus, only different internal pressures and punch head shapes were planned for the experiments. The dimensions of the tube, punch and die, such as the tube diameter, punch radius and die hole radius, were so chosen that the maximal internal pressure needed is smaller than 70 MPa, which is the safe capacity of the hydraulic power system used.

**Figure 14.** Main apparatus for hydro-flanging experiments.**Figure 15.** Appearance of die set and punch.

4.1. Experimental Results of Hydro-Flanging Processes

Table 4 shows the appearance of the hydro-flanged tubes and cross-sections at flanged regions under different internal pressures. The punch head height is $H_p = 4$ mm, the punch head radius is $r_p = 3.45$ mm and die hole radius is $r_h = 3.5$ mm. In case 1 ($P_i = 0$ MPa), fracture occurred at the bottom of the flanging region (zone A) and the aluminum alloy tube was pierced through by the punch with a large roll-over at a stroke of 15.6 mm. As the internal pressure increases, the roll-over or the gap height h_g decreases and the thickness at the ring zone increases. However, at $P_i = 50$ MPa and a stroke of 8 mm in case 4, necking occurs in zone B. As the internal pressure increases to 70 MPa in case 5, the flanging region broken in zone B separates completely from the ring zone. Generally speaking, the results in case 5 with a smaller roll-over and a about 3.4 mm-thick ring zone are beneficial for the subsequent inlaying process.

Table 4. Appearances of hydro-flanged tubes and cross-sections at flanged regions under different internal pressures.

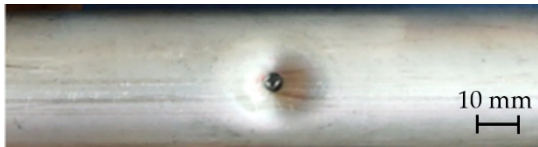
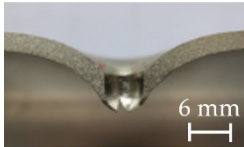


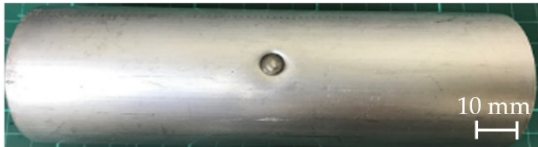

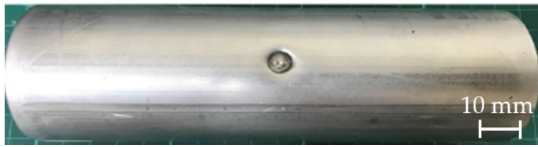
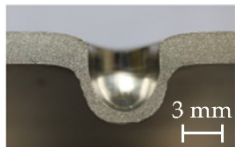
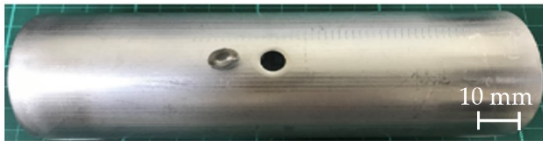
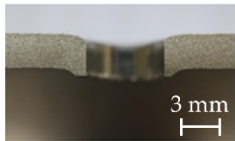
| Forming Conditions | Product Appearance | Cross-Sectional Appearance |
|---|--|---|
| Case 1 $P_i = 0$ MPa Stroke = 15.6 mm |  |  |
| Case 2 $P_i = 30$ MPa Stroke = 7 mm |  |  |
| Case 3 $P_i = 50$ MPa Stroke = 7 mm |  |  |
| Case 4 $P_i = 50$ MPa Stroke = 8 mm |  |  |
| Case 5 $P_i = 70$ MPa Stroke = 8 mm |  |  |

Figure 16 shows the experimental punch load variations for different internal pressures under $H_p = 4$ mm and $r_h = 3.5$ mm. It can be seen that the punch load increases significantly with the increase of internal pressure and the maximal load occurs earlier at a higher pressure. As the internal pressure is 70 MPa, the maximum punch load occurring at a stroke of 5.3 mm is about 11.4 kN. As the internal pressure is 50 MPa, the maximum punch load occurring at a stroke of 6.2 mm is about 9.1 kN. For $P_i = 30$ MPa, at a stroke of 7 mm, the punch load has not reached the maximal value yet.

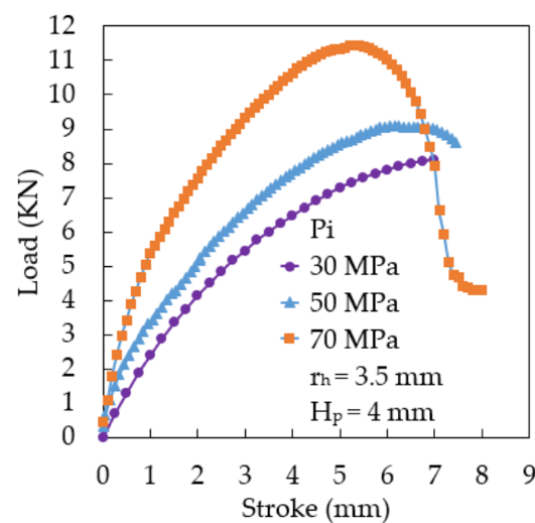


Figure 16. Experimental punch load variations for different internal pressures.

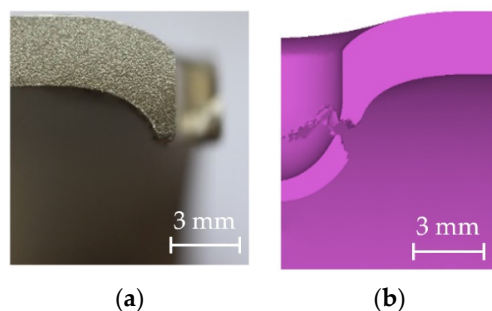
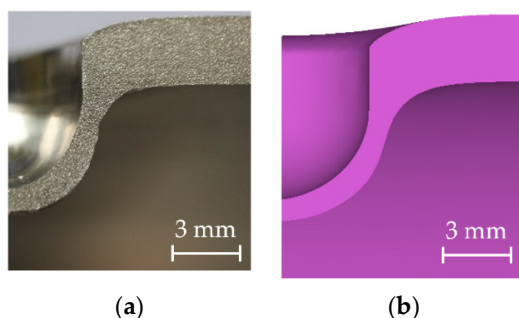
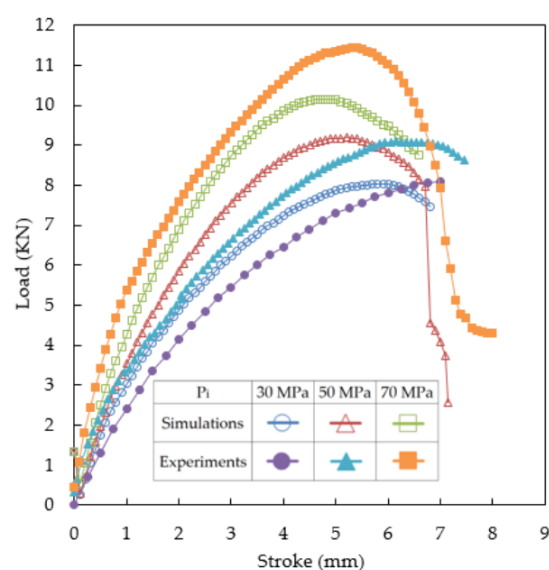
4.2. Comparisons of Simulative and Experimental Results

Table 5 shows the comparisons of thickness distributions at the flanging region between simulations and experiments. The punch height is fixed as $H_p = 4$ mm, the die hole radius is $r_h = 3.5$ mm and the stroke is 7 mm. It can be seen from the table that as the internal pressure increases, both the simulative and experimental thicknesses decrease. Generally, the differences between the simulation and experimental thicknesses were within 20%. The predicted fracture or necking positions were consistent with the simulation results. For $P_i = 30$ MPa, if the punch moves downward further, fracture occurs in zone B as shown in Figure 17. For $P_i = 50$ MPa, necking occurs in zone B as shown in Figure 18. The Normalized Cockcroft and Latham (NCL) ductile fracture criterion [21] was used to determine if the tube material reaches the fracture condition and the corresponding element is removed. The critical damage value was obtained by comparing the elongation and loading curve between the FE simulations and the real tensile tests. The obtained critical damage value for aluminum alloy A6063 is 0.63. The simulation result in Figure 17b showing tube fracture at the upper flanging region was obtained according to the NCL criterion adopted in “DEFORM3D” software.

Figure 19 shows the comparisons of the simulative and experimental punch load variations during hydro-flanging processes under $H_p = 4$ mm and $r_h = 3.5$ mm. The coefficient of friction used in the finite element simulations was $\mu = 0.3$, because a lot of new surface of the aluminum alloy tube generated at the flanging region during the hydro-flanging processes. It can be seen that the punch load increases with increasing internal pressures. For internal pressures of $P_i = 30$ MPa and 50 MPa, the simulative maximum loads are almost the same as the experimental values. For internal pressure of $P_i = 70$ MPa, some deviation of about 10% exists between the simulative and experimental maximal punch loads. For the maximal loads, generally the simulative values are close to the experimental data within an error of 10%. However, the forming moments or punch strokes corresponding to the maximal loads in the experiments occurred slightly later compared with the simulations. The reasons for the delay are probably because of the elastic deformation of the die and the compressibility of the hydraulic oil. During the finite element simulations, the punch and die were all assumed as rigid bodies and the compressibility of fluid media was not considered. During hydro-flanging, the load usually increases at the early stage and decreases at the late stage. A maximal value occurs as the whole punch head surface is in contact with the tube, as shown in Figures 11 and 12. For internal pressure of $P_i = 30$ MPa in the experiments, because of the delayed response of the load variation, the late stage for the decreasing period did not appear on the curve for the experiments with $P_i = 30$ MPa.

Table 5. Comparisons of thickness distributions at flanging region between simulation and experiment.

| $H_p = 4 \text{ mm}$ | | Simulation | | Experiment | | Difference | |
|----------------------|-----------------------------------|------------|--------|------------|--------|------------|--------|
| r_h | Z | 30 MPa | 50 MPa | 30 MPa | 50 MPa | 30 MPa | 50 MPa |
| 3.5 mm | t_2 ($z_2 = 2.5 \text{ mm}$) | 1.65 | 1.22 | 1.79 | 1.58 | −7.82% | −22.7% |
| | t_1 ($z_1 = 3.75 \text{ mm}$) | 1.43 | 1.27 | 1.51 | 1.41 | −5.29% | −9.93% |
| | t_0 ($z_0 = 5 \text{ mm}$) | 1.13 | 1.12 | 1.26 | 1.20 | −10.3% | −6.67% |
| | t_2/t_0 | 1.46 | 1.089 | 1.421 | 1.345 | 2.74% | −19.0% |

**Figure 17.** Cross-sectional configurations after hydro-flanging at $P_i = 30 \text{ MPa}$. (a) Experiment; (b) Simulation.**Figure 18.** Cross-sectional configurations after hydro-flanging at $P_i = 50 \text{ MPa}$. (a) Experiment; (b) Simulation.**Figure 19.** Simulative and experimental punch load variations during hydro-flanging.

5. Conclusions

In this study, a new hydro-flanging process was proposed to investigate the plastic deformation pattern of an aluminum alloy tube at the flanging region. A series of finite element simulations and experiments of hydro-flanging processes were carried out and some conclusions can be drawn as below:

- (1) As the internal pressure increased, the thickness of the tube at the bottom of the punch head became thinner. At a higher internal pressure, the tube was bulged up and, hence, the thickness close to the ring zone became thicker and that under the punch head became thinner.
- (2) A short blunt punch head made the thickness distribution more uniform and the thickness t_2/t_0 ratio was close to unity, which was more likely to result in fracture in zone B. If a long punch head was used instead, t_2/t_0 became larger, fracture would probably occur at zone A at the bottom of the punch head.
- (3) The change of punch hole radius r_h at a lower pressure did not affect the thicknesses at the flanging region; however, at a higher pressure of 70 MPa, the thicknesses decreased obviously as r_h increased.
- (4) The simulation results of thickness distributions and maximum punch loads were generally the same as the experimental results. Under a high internal pressure and a short blunt punch head, fracture was more likely to occur in zone B.

In this paper, the thickness distributions at the flanging region affected by the punch head shapes and internal pressures or loading paths were systematically discussed. In the future, bonding forces or holding forces of the inlaid nut from the ring zone for various hydro-flanged ring zone shapes during a nut hydro-inlaying process will be investigated.

Author Contributions: Conceptualization, methodology, research supervision and writing—review and editing were conducted by Y.-M.H. Simulations, experiments, were conducted by H.-N.P. Validation and writing—original draft preparation were completed by H.-S.R.T. All authors have read and agreed to the published version of the manuscript.

Funding: This research received a funding from the Ministry of Science and Technology of the Republic of China under Grant no. MOST 106-2221-E-110-029-MY3.

Institutional Review Board Statement: Not applicable.

Informed Consent Statement: Not applicable.

Data Availability Statement: Not applicable.

Acknowledgments: The authors would like to extend their thanks to the Ministry of Science and Technology of the Republic of China under Grant no. MOST 106-2221-E-110-029-MY3. The advice and financial support of MOST are greatly acknowledged.

Conflicts of Interest: The authors declare no conflict of interest.

References

1. Dohmann, F.; Hartl, C. Tube hydroforming—Research and practical application. *J. Mater. Process. Technol.* **1997**, *71*, 174. [[CrossRef](#)]
2. Ahmetoglu, M.; Altan, T. Tube hydroforming: State-of-the-art and future trends. *J. Mater. Process. Technol.* **2000**, *98*, 25. [[CrossRef](#)]
3. Fracz, W.; Stachowicz, F.; Trzepieciński, T. Investigations of thickness distribution in hole expanding of thin steel sheets. *Arch. Civ. Mech. Eng.* **2012**, *12*, 279–283. [[CrossRef](#)]
4. Kacem, A.; Krichen, A.; Manach, P.Y.; Thuillier, S.; Yoon, J.W. Failure prediction in the hole-flanging process of aluminum alloys. *Eng. Fract. Mech.* **2013**, *99*, 261–265. [[CrossRef](#)]
5. Liu, W.; Hao, J.; Liu, G.; Gao, G.; Yuan, S. Influence of punch shape on geometrical profile and quality of hole piercing-flanging under high pressure. *Int. J. Adv. Manuf. Technol.* **2016**, *86*, 1253–1262. [[CrossRef](#)]
6. Thipprakmas, S.; Jin, M.; Murakawa, M. Study on flanged shapes in fineblanked-hole flanging process using finite element method. *J. Mater. Process. Technol.* **2007**, *193*, 128–133. [[CrossRef](#)]
7. Mizumura, M.; Sato, K.; Kuriyama, Y. Development of nut-inlaying technique in hydroformed component by hydro-burring. *Mater. Trans.* **2012**, *53*, 801–806. [[CrossRef](#)]
8. Mizumura, M.; Sato, K.; Suehiro, M. Development of new hydroforming methods. *Nippon Steel Tech. Rep.* **2013**. Available online: <https://www.nipponsteel.com/en/tech/report/nsc/pdf/103-07.pdf> (accessed on 15 March 2021).

9. Choi, S.K.; Kim, W.T.; Moon, Y.H. Analysis of deformation surrounding a hole produced by tube hydro-piercing. *J. Eng. Manuf.* **2004**, *218*, 1091–1097. [\[CrossRef\]](#)
10. Hwang, Y.M.; Wu, R.K. Process and loading path design for hydraulic compound forming of rectangular tubes. *Int. J. Adv. Manuf. Technol.* **2017**, *91*, 2135–2142. [\[CrossRef\]](#)
11. Hwang, Y.M.; Dai, W.H.; Chen, C.C. Investigation of punch shape design in tube hydro-piercing processes. *Int. J. Adv. Manuf. Technol.* **2020**, *110*, 2211–2220. [\[CrossRef\]](#)
12. Hwang, Y.M.; Tsai, Y.J. Movable die and loading path design in tube hydroforming of irregular bellows. *Metals* **2020**, *10*, 1518. [\[CrossRef\]](#)
13. Park, J.Y.; Han, S.W.; Jeong, H.S.; Cho, J.R.; Moon, Y.H. Advanced sealing system to prevent leakage in hydroforming. *J. Mater. Process. Tech.* **2017**, *247*, 103–110. [\[CrossRef\]](#)
14. Yu, X.Y.; Chen, J.; Chen, J.S. Interaction Effect of Cracks and Anisotropic Influence on Degradation of Edge Stretchability in Hole-expansion of Advanced High Strength Steel. *Int. J. Mech. Sci.* **2016**, *105*, 348–359. [\[CrossRef\]](#)
15. Kumar, S.; Ahmed, M.; Panthi, S.K. Effect of Punch Profile on Deformation Behaviour of AA5052 Sheet in Stretch Flanging Process. *Arch. Civil Mech. Eng.* **2020**, *20*, 1–17. [\[CrossRef\]](#)
16. Dixit, U.S.; Joshi, S.N.; Davim, J.P. Incorporation of material behavior in modeling of metal forming and machining processes: A review. *Mater. Des.* **2011**, *32*, 3655–3670. [\[CrossRef\]](#)
17. Del Pozo, D.; López de Lacalle, L.N.; López, J.M.; Hernández, A. Prediction of press/die deformation for an accurate manufacturing of drawing dies. *Int. J. Adv. Manuf. Technol.* **2008**, *37*, 649–656. [\[CrossRef\]](#)
18. Fernández-Abia, A.I.; Barreiro, J.; López de Lacalle, L.N.; Martínez-Pellitero, S. Behavior of austenitic stainless steels at high speed turning using specific force coefficients. *Int. J. Adv. Manuf. Technol.* **2012**, *62*, 505–515. [\[CrossRef\]](#)
19. Hwang, Y.M.; Pham, H.N. Study of Hydro-Reaming and Flanging of Aluminum Tubes. Tube Hydroforming Technology. In Proceedings of the 9th International Conference on Tube Hydroforming, Kaohsiung, Taiwan, 18–21 November 2019; pp. 124–129.
20. ASTM. *Standard Test Methods for Tension Testing of Metallic Materials*; E8/E8M-15; ASTM International: West Conshohocken, PA, USA, 2015; pp. 10–11.
21. Oh, S.I.; Chen, C.C.; Kobayashi, S. Ductile fracture in axisymmetric extrusion and drawing. *ASME J. Eng. Ind.* **1979**, *101*, 36–44. [\[CrossRef\]](#)